EPJ Web of Conferences **292**, 01002 (2024) https://doi.org/10.1051/epjconf/202429201002
*NRM2023*

# Nuclear reactions as a tool to study the microscopic structure of pygmy and giant resonances

*Nadia* Tsoneva[1,*]

[1]Extreme Light Infrastructure (ELI-NP), Horia Hulubei National Institute for R&D in Physics and Nuclear Engineering (IFIN-HH), Str. Reactorului No. 30, 077125 Bucharest-Măgurele, Romania

**Abstract.** An advanced microscopic approach based on energy-density functional theory and the quasiparticle-phonon model has been used to study nuclear excitations up to giant dipole resonance energies. In addition, our nuclear structure model has been extended to include reaction theory. The theoretical spectral distributions compared with experimental data performed with different probes and techniques are able to provide us with information about the microscopic structure of the pygmy dipole resonance as well as its collectivity. Evaluations of electric dipole (E1) transition strengths and branching ratios at low energy reveal different properties of the nuclear excitations and the effect of quasi-continuum coupling. The present studies will support above-neutron-threshold $\gamma$ experiments at ELI-NP targeting $\gamma$ decays of giant and pygmy resonances, as well as studies on multi-step $\gamma$ decays by low-lying states.

## 1 Introduction

At nuclear excitation energies below the neutron separation energy, excitation modes of different origins exist, making the interpretation of low-energy nuclear spectra a difficult task. In recent years, new nuclear excitation modes closely related to skin phenomena in atomic nuclei, called pygmy dipole resonance (PDR) [1–10] and its natural extension at higher multipolarities - the pygmy quadrupole resonance (PQR) [11–13] have been theoretically and experimentally observed and investigated. These studies show that understanding low-energy nuclear spectra, and in particular pygmy resonances, requires the application of various probes and experimental techniques, as well as advanced microscopic theoretical methods. In addition, pygmy resonances have been found to be important for understanding fundamental properties of the nucleus and nuclear matter such as nuclear skin thickness and symmetry energy, as well as for nuclear astrophysics and the nucleosynthesis of heavier elements in the Universe [14–17]. We must emphasize that there is currently no direct method for experimentally determining neutron skin thickness from nuclear spectral measurements. However, the distinction between pygmy and other modes can be made theoretically, and the derived pygmy dipole strengths can be used to quantify the neutron skin thickness [5, 14, 18].
In this manuscript, we report our recent theoretical studies of the nuclear electric dipole response in magic and semi-magic nuclei from different nuclear mass regions, which are particularly important to understand the fine and coarse spectral features of low-energy dipole spectra and the observed relationship between the PDR and neutron skin thickness [3, 6, 19].

*e-mail: nadia.tsoneva@eli-np.ro

The theoretical results are obtained within the framework of the Energy-Density Functional (EDF) and Quasiparticle-Phonon Model (QPM) approach [5, 6, 19, 20]. A common observation in these studies is, that the quasiparticle-random-phase-approximation (QRPA) is not sufficient to describe the nuclear excitations below the neutron threshold [5, 6, 21]. The systematic comparison in various nuclei between EDF+QRPA (EQRPA) and the three-phonon EDF+QPM (EQPM) calculations shows that the behavior of the low-energy dipole strength is influenced by the competition between static and dynamical effects. The first one is related to the mean-field (MF) and the PDR associated with neutron skin oscillations, while the second one represents the coupling of the single-particle states with a more complex excitations related to core polarization and giant dipole resonance (GDR) [14, 21]. These effects lead to the redistribution and fragmentation of the low-energy dipole strength. We should emphasize that the neutron $1p-1h$ components of the dipole spectral distributions are of particular importance, since they have been identified as possible doorway states shared between neutron and $\gamma$ channels in $(n,\gamma)$ reactions [22]. As doorway states, the $1^-$ states of the PDR, which are mostly of $1p-1h$ neutron character, are expected to strongly influence $(n,\gamma)$ cross sections and thereby affect isotope production in explosive stellar environments [17]. In this context, we will present our recent study on $^{208}$Pb$(d,p)$ and $^{120}$Sn$(d,p\gamma)$ reactions, which explains the population mechanism of the neutron $1p-1h$ components entering the state vectors of the PDR $1^-$ states [22, 23].

Furthermore, the electric dipole strength below the neutron separation energy can be strongly influenced by contributions from the fragmented dipole strength of $1^-$ excited states in the quasicontinuum region, which can greatly increase the electric dipole strength below the neutron threshold. Our theoretical results in $^{204}$Pb observed a strong influence of the quasicontinuum to the total electric dipole strength below the neutron threshold [24].

Another interesting case that we recently investigated is the neutron-rich $^{206}$Pb (N/Z=1.51) nucleus which is expected to have a robust neutron skin and, as a consequence, an additional low-energy dipole strength associated with skin dynamics. Furthermore, the presence of the PDR mode in $^{206}$Pb can significantly affect the $^{205}$Pb radiative neutron capture cross section, a reaction associated with the synthesis of $^{206}$Pb during s-process [14]. The role of PDR for the nucleosynthesis of heavier elements related to the s-process of nucleosynthesis we have also been systematically investigated in the N=50 isotones [17].

## 2 Theoretical approach: EQPM and Reaction Theory

Recently, we have developed a novel approach that combines the EQPM theory [6, 19, 20] with a nuclear reaction model (EQPM + Reaction). The method successively integrates the nuclear structure in the reaction theory to calculate the differential $(d,p)$, $(d,p\gamma)$ and $(\alpha,\alpha'\gamma)$ cross sections, and $\gamma$-decay branchings and energy-integrated $(\gamma,\gamma')$ cross-sections [22, 23, 31]. Our studies of the $^{207}$Pb(d,p)$^{208}$Pb and $^{119}$Sn(d, p$\gamma$)$^{120}$Sn reaction cross sections show the population of only selected $1^-$ states with a specific microscopic structure that are located in a limited energy range below the neutron threshold. Furthermore, our observations indicate that the understanding of the microscopic structure of the $1^-$ states at low energies is crucial for correctly modeling their population in nuclear reactions and their subsequent decay, which in turn raises questions about the applicability of statistical approaches to (n, $\gamma$) reactions in the PDR region.

In the last years the method was implemented in studies of the properties of nuclear electric and magnetic excitations in the PDR region and it was found very successful for description of the low-energy $\gamma$-strength functions and more particularly of the PDR [6, 8, 25]. An important advantage of the EQPM approach is the description of the nuclear excitations in terms of QRPA phonons as a building blocks of the three-phonon QPM model space [26, 27] which

provides a microscopic way to multi-configuration mixing. Thus, the EQPM allows for sufficiently large configuration spaces which is required for a unified description of low-energy single- and multi-particle states and also for the GDR energy region.

The model Hamiltonian is given by:

$$H = H_{MF} + H_{res}, \tag{1}$$

where $H_{MF}$ is a mean-field part and $H_{res}$ stands for the residual interaction.

The mean-field (MF) part $H_{MF}$ is treated by self-consistent Skyrme Hartree-Fock-Bogoliubov (HFB) theory described in [6, 28]. The pure HFB picture is in fact extended beyond MF by dynamical self-energies, hence incorporating a more detailed spectral description of nuclear spectra. The procedure allows us to account in a self-consistent manner for nuclear binding energies and other ground-state properties of nuclei like the charge radii and the neutron skin thickness and to reproduce precisely the results obtained from Skyrme SLy4HFB calculations [5] and available experimental data [6, 28].

The nuclear excited states are calculated with a residual interaction which is based on the QPM formalism [26]:

$$H_{res} = H_M^{ph} + H_{SM}^{ph} + H_M^{pp}, \tag{2}$$

where effective interactions are implemented to account for the interaction between the quasiparticles. The terms $H_M^{ph}$, $H_{SM}^{ph}$ and $H_M^{pp}$ are taken as a sum of isoscalar and isovector separable multipole and spin-multipole interactions in the particle-hole $(p-h)$ and multipole pairing interaction in the particle-particle $(p-p)$ channels, respectively [26]. The model parameters are fixed empirically in such a way that the properties of the lowest-lying collective states and giant resonances are described accurately [20]. An exception is the isovector spin-dipole coupling constant, which is obtained from fully self-consistent QRPA calculations using the microscopic EDF of Ref. [28].

The QPM formalism allows for a further expansion of QRPA $p-h$ excitations to multi-particle-multi-hole states in terms of coupling between quasiparticles and phonons [26].

The QRPA phonons are defined with the equation

$$Q^+_{\lambda\mu i} = \frac{1}{2}\sum_{j_1 j_2}^{\tau=n,p} \left(\psi^{\lambda\mu i}_{j_1 j_2} A^+_{\lambda\mu}(j_1 j_2) - \varphi^{\lambda\mu i}_{j_1 j_2} \widetilde{A}_{\lambda\mu}(j_1 j_2)\right) \tag{3}$$

where $j \equiv (nlj)$ is a single-particle proton or neutron state with a magnetic quantum number $m$ and an isospin $\tau$, $A^+_{\lambda\mu}(j_1 j_2) = \left[\alpha^+_{j_1}\alpha^+_{j_2}\right]_{\lambda\mu}$ and the time reversed operator $\widetilde{A}_{\lambda\mu} = (-)^{\lambda-\mu} A_{\lambda-\mu}$, where $A_{\lambda\mu}(j_1 j_2) = \left[\alpha_{j_1}\alpha_{j_2}\right]_{\lambda\mu}$, are (bare) two-quasiparticle creation and annihilation operators defined by coupling of two one-quasiparticle operators to total angular momentum $\lambda$ with projection $\mu$: $[\alpha^+_{j_1}\alpha^+_{j_2}]_{\lambda\mu} = \sum_{m_1 m_2} C^{\lambda\mu}_{j_1 m_1 j_2 m_2}\alpha^+_{j_1 m_1}\alpha^+_{j_2 m_2}$. The quasiparticle creation $\alpha^+_{jm}$ and annihilation $\alpha_{jm}$ operators are defined with the canonical Bogolyubov transformation of nucleon creation $a^+_{jm}$ and annihilation $a_{jm}$ operators, taken in standard form $a_{jm} = u_j\alpha_{jm} + (-1)^{j-m}v_j\alpha^+_{j-m}$, where $u_j$ and $v_j$ are nucleon occupation probabilites [26].

The QRPA operators obey the equation of motion

$$[H, Q^+_\alpha] = E_\alpha Q^+_\alpha, \tag{4}$$

which solves the eigenvalue problem, giving the excitation energies $E_\alpha$ and the time-forward and time-backward amplitudes $\psi^{\lambda i}_{j_1 j_2}$ and $\varphi^{\lambda i}_{j_1 j_2}$, respectively.

The QPM phonon operators satisfy exact commutation relations between phonons and quasiparticles which preserve the fermion structure of the phonon operators [20, 29].

For spherical even-even nuclei the model Hamiltonian is diagonalized on an orthonormal set of wave functions constructed from one-, two- and three-phonon configurations [20, 27]:

$$\Psi_\nu(JM) = \left\{ \sum_i R_i(J\nu) Q^+_{JMi} + \sum_{\substack{\lambda_1 i_1 \\ \lambda_2 i_2}} P^{\lambda_1 i_1}_{\lambda_2 i_2}(J\nu) \left[ Q^+_{\lambda_1\mu_1 i_1} \times Q^+_{\lambda_2\mu_2 i_2} \right]_{JM} \right.$$
$$\left. + \sum_{\substack{\lambda_1 i_1 \lambda_2 i_2 \\ \lambda_3 i_3 I}} T^{\lambda_1 i_1 \lambda_2 i_2 I}_{\lambda_3 i_3}(J\nu) \left[ \left[ Q^+_{\lambda_1\mu_1 i_1} \otimes Q^+_{\lambda_2\mu_2 i_2} \right]_{IK} \otimes Q^+_{\lambda_3\mu_3 i_3} \right]_{JM} \right\} \Psi_0 \tag{5}$$

where R, P and T are unknown amplitudes, and $\nu$ labels the number of the excited states.

The electromagnetic transition matrix elements are calculated for transition operators including the interaction of quasiparticles and phonons [29] where exact commutation relations are implemented which is a necessary condition in order to satisfy the Pauli principle.
The nuclear spectroscopic information obtained within the framework of the EQPM theory such as occupation numbers, quasiparticle and phonon amplitudes, spectroscopic factors, transition densities and spectral functions [26] can be further implemented into a nuclear reaction model (EQPM + Reaction) to consistently derive the different nuclear reaction cross sections [6, 17, 22, 23, 31, 32].

## 3 Discussion

### 3.1 Microscopic structure of the Pygmy Dipole Resonance in $^{208}$Pb

The first detailed investigation of the one-particle character of the PDR in $^{208}$Pb based on new experimental data and its theoretical explanation is discussed in Ref. [22]. Theoretical predictions from EQPM and Large-Scale-Shell-Model (LSSM) are compared with novel data from (d,p) and resonant proton scattering experiments performed at the Q3D spectrograph of Maier-Leibnitz-Laboratory in Garching, Germany. Two different transfer configurations through which $1^-$ states of $^{208}$Pb can be populated from the $J^\pi=1/2^-$ ground state of $^{207}$Pb have been distinguished; namely $(3p_{1/2})^{-1}(4s_{1/2})^{+1}$ (l=0), and $(3p_{1/2})^{-1}(3d_{3/2})^{+1}$ (l=2). The measured angular distributions are found in excellent agreement with Distorted-Wave-Born-Approximation (DWBA) model calculations [22]. In addition, the detailed, high-resolution (d,p) experimental study of the PDR in $^{208}$Pb is supplemented with available experimental data to discuss the microscopic structure of the PDR by comparing it to the state-the-art theoretical models: EQPM and LSSM [22]. The neutron $1p-1h$ configurations that contribute to the formation of the PDR are accessed from (d,p) data up to the proton separation energy $S_p$ and for a limited number of states from the results of resonant proton scattering via isobaric analog resonances $(p,p')_{IAR}$, which probes components that could not be populated in the selective one-neutron transfer reaction [22]. The model-independent, angle-integrated (d,p) cross-sections and $C_{LJj}$ amplitudes from $(p,p')_{IAR}$ are shown in Fig.1 in comparison to a selection of other experimental data on the PDR in $^{208}$Pb [22]. The (d,p) strength pattern [Fig. 1(a)] is dominated by the two strongly populated $1^-$ states at 5292 and 5947 keV, corresponding to the major fragments of the $(3p_{1/2})^{-1}(4s_{1/2})^{+1}$ [S=0.77(4)] and $(3p_{1/2})^{-1}(3d_{3/2})^{+1}$ [S=0.66(4)] neutron $1p-1h$ strength, respectively. Figures 1(c,d,e,f) present the results of EQPM and LSSM calculations [22]. The differential cross-sections $d\sigma/d\Omega$, predicted theoretical spectroscopic factors, i.e., the overlap of the $^{207}$Pb ground state with excited $1^-$ states in $^{208}$Pb when adding a neutron, were combined with the DWBA calculations. Unprecedented access to the theoretical wave functions demonstrating the $1p-1h$ neutron origin of the

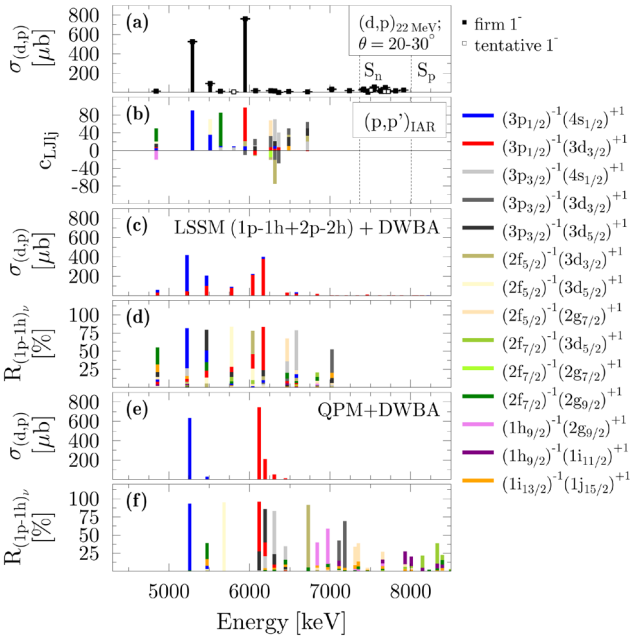


**Figure 1.** (Color online) (a) Angle-integrated (d,p) cross-sections $\sigma$(d,p). (b) $C_{LJij}$ amplitudes from $(p, p')_{IAR}$. (c) $\sigma$(d,p) predicted by combining LSSM spectroscopic factors with DWBA calculations. (d) Decomposition of the LSSM wave functions into neutron $1p-1h$ components relative to the total wave function $\Psi_{total}$.(e), (f) same as (c), (d) but for EQPM [22].

PDR in $^{208}$Pb has been achieved. In particular, EQPM predicts a dominant $(3p_{1/2})^{-1}(4s_{1/2})^{+1}$ [$S_{5.32MeV}$=0.92] fragment and in agreement with experiment, the $(3p_{1/2})^{-1}(3d_{3/2})^{+1}$ strength to be mainly concentrated in one state [$S_{6.12MeV}$=0.68]. The total (d,p) cross-section value, obtained from the EQPM theory is $\Sigma\sigma_{(d,p)(QPM)}$= 1676 $\mu$b. It is found in very good agreement with the total experimental (d,p) cross-section value which can be taken as a sum of $\sum_{\leq S_n}\sigma_{(d,p)(exp.)}$= 1524(17) $\mu$b below and $\sum_{\geq S_n}\sigma_{(d,p)(exp.)}$= 254(9) above the neutron threshold $S_n$, respectively. However, also the QPM does not fragment the l=0 and l=2 strength sufficiently to describe the strength above $S_n$.

### 3.2 Microscopic structure of the Pygmy Dipole Resonance in $^{120}$Sn

The one-particle character of the PDR in semi-magic $^{120}$Sn based on EQPM+Reaction approach and novel measurements of the $^{119}$Sn(d,p$\gamma$)$^{120}$Sn reaction cross section, performed at the University of Cologne with the combined SONIC@HORUS setup for coincident particle-spectroscopy, is discussed in [23]. In contrast to the case of the double-magic $^{208}$Pb nucleus [22], the PDR in an open-shell nucleus $^{120}$Sn is characterized by a much higher level density. In order to describe the observed fragmentation pattern of the PDR mode in semi-magic nucleus $^{120}$Sn, one must go beyond QRPA and to take into account the interaction between quasiparticles and phonons. That is achieved by the three-phonon QPM approach. The theoretical results of (d,p$\gamma$) yields, and energy-integrated ($\gamma$, $\gamma'$) cross-sections in $^{120}$Sn obtained from the three-phonon QPM calculations are shown in Fig.2. Below 7 MeV, one-phonon PDR configurations dominate the spectral distributions, while above 7 MeV, GDR and more complex configurations predominate. The theoretical observations are found in very good agreement with the novel (d,p$\gamma$) experiment from Ref. [23]. The theoretical (d,p$\gamma$) strength is

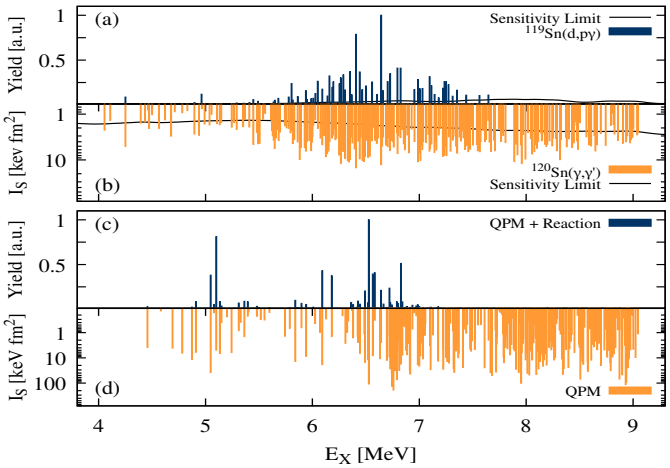


**Figure 2.** (Color online.) (*a*) relative $\gamma$-ray yields from $^{119}Sn(d, p\gamma)$ and (*b*) energy integrated cross sections $I_S$ for $^{120}Sn(\gamma, \gamma')$. All transitions shown in panel (*a*) were also observed in the NRF experiment. Sensitivity limits are based on a maximum error on the peak area of 30%. (*c*) relative $^{119}Sn(d, p\gamma)$ yields from the EQPM+Reaction formalism and (*d*) predicted energy integrated cross sections, both taking into account $\gamma$-decay branching predicted by the EQPM. Theoretical $(d, p)$ cross sections were calculated at scattering angles identical to the experiment. Experimental and theoretical yields were normalized to the strongest transition, respectively [23].

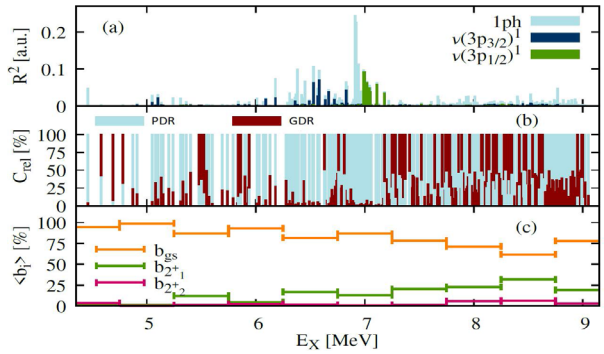


**Figure 3.** Summed squared one-phonon $R$ amplitudes for each QPM state, representing the contribution of a given configuration to the QPM wave function (5). Individual contributions of neutron $1p - 1h$ configurations accessible in $^{119}Sn(d, p)$ are shown in *dark blue* and *green*, respectively. (*b*) shows the ratio $C_{rel}=\sum R^2_{PDR}/\sum(R^2_{PDR} + R^2_{GDR})$. (*c*) $\gamma$-decay branching to the ground state and to the two lowest-lying excited $2^+$ states in $^{119}$Sn, averaged over all states in a window of 500 keV.

fragmented at lower energies and it reproduces the experimental centroid energy of 6.49 MeV as well as summed $(\gamma,\gamma')$ cross-sections for states excited with both probes: $\sum I_S^{QPM}$=243 keV fm$^2$ and $\sum I_S^{QPM}$=360 keV fm$^2$ for states with a theoretical relative (d,p$\gamma$) yield larger than 1% and 0.5%, respectively. Experimentally, a summed energy-integrated cross section of $\sum I_S^{NRF}$=337 keV fm$^2$ [23].

A careful analysis of the EQPM results which are shown in Fig. 3 revealed that the currently discussed structural change in the entire PDR region, which partially causes the discrepancy

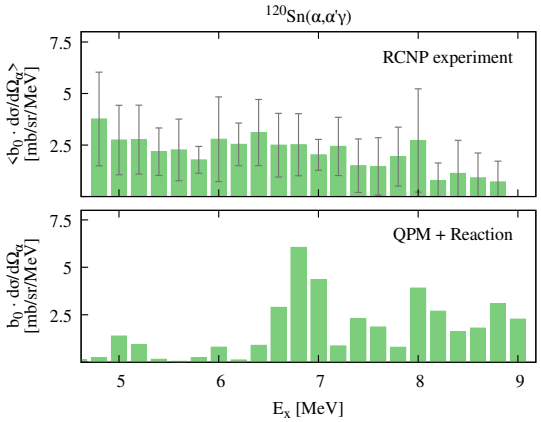


**Figure 4.** Top: Experimental $^{120}$Sn$(\alpha, \alpha'\gamma)$ integrated ground-state decay cross sections in 500 keV bins between 5 MeV and 9 MeV. Error bars indicate statistical errors only. Bottom: EQPM+Reaction calculations [31]. For a consistent comparison between experiment and theory, absolute differential cross sections $\frac{d\sigma}{d\Omega_\alpha}$ integrated over the spectrometer solid angle $\Omega_\alpha$ and folded with the ground-state decay branching-ratio $b_0$, were extracted from the EQPM calculations [30, 31].

between $(p, p')$ and $(\gamma, \gamma')$ experiments, is actually predicted by the EQPM [23]. As seen in Fig. 3 $(b)$ and $(c)$, the $\gamma$-decay behavior of the $1^-$ states does indeed change as the states' structure becomes more complex with the average ground-state branching ratio decreasing and the average ratios to excited states increasing. This underlines the need for comparing experimental data and theoretical calculations on the same footing as done here by limiting the comparison to configurations selectively populated in $(d, p)$, ground-state $\gamma$ decays, and comparing the true experimental NRF observable to the consistently calculated EQPM quantity. The selective population of only the lower group of states in $(d, p\gamma)$ shows the importance of a consistent description of structure and reaction theory.

To investigate the structure of the PDR in more detail, further experiments with complementary probes are necessary. The $(\alpha, \alpha'\gamma)$ reaction at intermediate energies is an excellent tool for studying low-spin states and E1 strength, similar to NRF [1]. Fig. 4 shows theoretical calculations carried out in the EQPM+Reaction theory that allow one to distinguish between isoscalar and isovector contributions to each $1^-$ state based on the proton and neutron transition densities derived from the EQPM [5, 31]. Integrated theoretical and experimental $(\alpha, \alpha'\gamma)$ cross sections are found in good agreement [30, 31].

## 4 Conclusions

The presented EQPM+Reaction studies have proved the neutron single-particle origin of PDR in the magic $^{208}$Pb and semi-magic $^{120}$Sn nucleus, which was confirmed by comparison with novel experimental data. Furthermore, the obtained results established (d,p), (d,p$\gamma$) and $(\alpha, \alpha'\gamma)$ reactions as additional, valuable experimental probes to study the microscopic structure of PDR, its isospin content and collectivity. This is achieved through unprecedented access to theoretical wave functions. Our theoretical studies of branching ratios and E1 spectral distributions in $^{120}$Sn, $^{204}$Pb and other nuclei show a strong influence of the quasicontinuum on the total electric dipole strength below the neutron threshold. This finding is important in explaining the long-standing controversy between inelastic $\gamma$ and proton scattering data for the observed dipole strength below the neutron threshold. Furthermore, the

applications of EQPM approach in astrophysical studies confirmed that knowledge of the microscopic structure PDR is important for accurately determining neutron capture reaction rates for astrophysics.

## Acknowledgement

This work was carried out under the contract PN 23.21.01.06 sponsored by the Romanian Ministry of Research, Innovation and Digitalization.

## References

[1] D. Savran *et al.*, Prog. Part. Nucl. Phys. **70**, 210 (2013)and refs. therein
[2] A. Bracco *et al.*, Eur. Phys. J. A **51**: 99 (2015) and refs. therein
[3] N. Tsoneva, H. Lenske, Ch. Stoyanov, Phys. Lett. B **586**, 213 (2004)
[4] S. Volz *et al.*, Nucl. Phys. A **779**, 1 (2006)
[5] N. Tsoneva, H. Lenske, Phys. Rev. C **77**, 024321 (2008) and refs. therein
[6] N. Tsoneva, H. Lenske, Phys. Atom. Nucl. **79**, 885–903 (2016) and refs. therein
[7] R. Schwengner *et al.*, Phys. Rev. C **78**, 064314 (2008)
[8] A. P. Tonchev *et al.*, Phys. Rev. Lett. **104**, 072501 (2010)
[9] R. Schwengner *et al.*, Phys. Rev. C **87**, 024306 (2013)
[10] Krishichayan *et al.*, Phys. Rev. C **91**, 044328 (2015)
[11] N. Tsoneva, H. Lenske, Phys. Lett. B **695**, 174 (2011)
[12] L. Pellegri *et al.*, Phys. Rev. C **92**, 014330 (2015)
[13] M. Spieker *et al.*, Phys. Lett. B, **752**, 102 (2016)
[14] A. P. Tonchev *et al.*, Phys. Lett. B **773**, 20 (2017)
[15] S. Goriely and E. Khan, Nucl. Phys. A **706**, 217 (2002)
[16] R. Raut *et al.*, Phys. Rev. Lett. **111**, 112501 (2013)
[17] N. Tsoneva *et al.*, Phys. Rev. C **91**, 044319 (2015) and refs. therein
[18] A. Tamii *et al.*, Phys. Rev. Lett. **107** 062502 (2011)
[19] H. Lenske and N. Tsoneva, Eur. Phys. J. A, **55**, 238 (2019)
[20] M. Grinberg, Ch. Stoyanov, N. Tsoneva, Phys. Elem. Part. At. Nucl., vol. **29**, part 6, 1456 (1998)
[21] N. Tsoneva, H. Lenske, J. Phys.: Conf. Ser. **366**, 012043 (2012)
[22] M. Spieker *et al.*, Phys.Rev.Lett. 125, 102503 (2020) and refs. therein
[23] M. Weinert *et al.*, Phys. Rev. Lett. **127**, 242501 (2021) and refs. therein
[24] T. Shizuma *et al.*, Phys. Rev. C 106, 044326 (2022)
[25] G. Rusev *et al.*, Phys. Rev. Lett. **110**, 022503 (2013)
[26] V. G. Soloviev, *Theory of complex nuclei* (Oxford: Pergamon Press, 1976)
[27] M. Grinberg, Ch. Stoyanov, Nucl. Phys. A **573** 231 (1994)
[28] F. Hofmann and H. Lenske, Phys. Rev. C **57**, 2281 (1998)
[29] V. Yu. Ponomarev *et al.*, Nucl. Phys. A **635**, 470 (1998)
[30] M. Weinert, PhD Thesis, University of Cologne (2022)
[31] M. Weinert, E.G. Lanza, N. Tsoneva *et al.*, to be submitted
[32] E.G. Lanza *et al.*, Prog. Part. Nucl. Phys., Vol. **129**, 104006 (2023)